Empirical Tight-Binding Calculation of Electronic Structure of Mn-Doped ZnS Nanocrystals

Rutchapon Hunkao[1], Sujin Suwanna[1], Worasak Sukkabot[2,*]

[1] Optical and Quantum Physics Laboratory, Department of Physiscs, Faculty of Science, Mahidol University,Bangkok,10400 Thailand

[2] Department of Physiscs, Faculty of Science, Ubon Ratchathani University, Ubon Ratchathani 34190, Thailand

[*] E-mail: w.sukkabot@gmail.com *Tel*. +66 8 8013 7387

Abstract

We investigate the electronic structure of Mn-doped ZnS nanocrystals using empirical tight-binding calculation. Such nanocrystals have been identified for many applications such as LEDs, electroluminescence devices, and sensors. By numerically solving the tight-binding Hamiltonian for wave functions and energies in the basis of linear combinations of atomistic orbitals, we obtain the electrons and holes energy levels, as well as the energy gap as the Mn doping concentration increases. Our results agree very well with other tight-binding calculations, and consistent with those from experiments. In particular, the energy gap decreases as the Mn doping concentration increases, with the results being more pronounced for smaller nanocrystal sizes.

Keywords: Mn-doped ZnS nanocrystal, band gap, tight-binding calculation.

Introduction

ZnS is a luminescent material that has been used for many applications such as light-emitting diodes (LEDs), electroluminescence devices, flat panel displays, sensors, lasers, infrared windows, solar cells and bio-devices [1]. The absorption and photoluminescence (PL) emission spectra can be tuned with particle sizes [2], [3], shape [4] and doping materials [5] due to quantum confinement effect. The electrons adjust their energies corresponding to boundaries when the particle size is comparable to electron wavelength. By doping Mn into ZnS nanocrystals, the luminescence efficiency enhances, and the lifetime shortens in comparison with the bulk material [6-7]. Mn-doped ZnS is an example of II-VI diluted magnetic semiconductors, which exhibit ferromagnetic properties with useful semiconductor properties being preserved. This material is a promising candidate as spintronic device where an electron spin is exploited as an additional degree of freedom. For instance, in quantum computing, a spin polarized electron localized in a quantum dot can be used as a quantum bit. The key feature is to control spins. Due to the strong *sp-d* exchange interaction between localized spins and carriers, the spin polarization can be generated through the giant Zeeman effect by an external magnetic field. These features have been successfully implemented in a spin filter [8] and a spin-polarization generator [9], [10].

Due to the benefit of the quantum confinement and spintronics, the dilute magnetic nanocrystals are the prospective candidates. Owing to the high computational demand of the first-principle and pseudo-potential calculation, a tight-binding model is an outstanding approach to study the dilute magnetic nanocrystals with experimentally synthesized sizes. This model is powerful in terms of electronic structure and density of states calculation, which is benchmarked consistently with first-principle calculation and requires much less computational resource. More details of computational formulation, accuracy, efficiency and applicability to various physical systems can be found, for example, in Ref. [11].

In this work, we study the effects of Mn doping into ZnS nanocrystals on the electronic structure and density of states (DOS) of ZnS using empirical tight-binding calculation. Here, the atomistic models are proposed for these calculations. Moreover, we include the *sp-d* exchange interaction by using mean-field approximation and show its effects on the electronic structure and DOS. The paper is organized in the following. Sections 2 and 3 describe the theoretical methodology used to construct the atomistic model for our tight-binding calculation, and simulation procedure. The simulation results are mainly analyzed and discussed in Section 4, followed by the summary and conclusion in Section 5

Theory and related work

Tight-Binding Model

For quantitative analysis of Mn-doped ZnS nanocrystals, a simple but effective computational model based on the atomistic tight-binding theory is proposed to investigate the electronic structure and DOS. In the present study, the $sp^3d^5s^*$ tight-binding model with the first-nearest neighbor interaction is used in conjunction with the spin-orbital coupling to simulate the electronic wave functions and associate energies in Mn-doped ZnS nanocrystals with the zinc-blende structure. The carrier wave function is given by a linear combination of atomistic orbitals α, localized on each atom β, as defined by

$$\psi = \sum_{\beta}^{N}\sum_{\alpha}^{20} C_{R,\alpha}\,\varphi_{\alpha}(\vec{r}-\vec{R}_{\beta}) \qquad (1)$$

where N is the total number of atoms. To obtain the single-particle spectra, the empirical tight-binding Hamiltonian H_{TB} is diagonalized numerically, where

$$H_{TB} = \sum_{\beta=1}^{N}\sum_{\alpha=1}^{20}\varepsilon_{\beta,\alpha}c^{\dagger}_{\beta\alpha}c_{\beta\alpha} + \sum_{\beta=1}^{N}\sum_{\alpha=1}^{20}\sum_{\alpha'=1}^{20}\lambda_{R\alpha\alpha'}c^{\dagger}_{\beta\alpha}c_{\beta\alpha'} + \sum_{\beta=1}^{N}\sum_{\beta'=1}^{N}\sum_{\alpha=1}^{20}\sum_{\alpha'=1}^{20}t_{\beta\alpha,\beta'\alpha'}c^{\dagger}_{\beta\alpha}c_{\beta'\alpha'} \qquad (2)$$

In Eq. (2), the operator $c^{\dagger}_{\beta\alpha}(c_{\beta\alpha})$ creates (annihilates) the particle on the orbital α of atom β. Here, $\varepsilon_{R\alpha}$, $\lambda_{R\alpha\alpha'}$ and $t_{R\alpha,R'\alpha'}$ are the on-site empirical parameters, the spin-orbit coupling constant and the off-site empirical parameters given in Table 1; see also Ref.[12]. While doped Mn parameters of sp^3s^* orbital basis are kept the same for ZnS, but the *d* orbital parameters are chosen as following Ref.[13]: $sd\sigma = -3.16\ \text{eV}$, $pd\sigma = -2.95\ \text{eV}$, $pd\pi = 1.36\ \text{eV}$ and $Ed = -6.45\ \text{eV}$. The hopping parameters V

Table 1. Tight-binding parameters of ZnS bulk semiconductors [12] with a and c denoting anion and cation, respectively.

Hopping parameters	$4V_{s,s}$	$4V_{x,x}$	$4V_{x,y}$	$4V_{s,p}$	$4V_{p,s}$	$4V_{s^*,p}$	$4V_{p,s^*}$
(eV)	-6.30	3.11	5.00	5.16	5.17	2.89	1.75

Onsite-energy	$\varepsilon_{s,a}$	$\varepsilon_{p,a}$	$\varepsilon_{s,c}$	$\varepsilon_{p,c}$	$\varepsilon_{s^*,a}$	$\varepsilon_{s^*,c}$	λ_a	λ_c
(eV)	-11.61	1.48	1.11	6.52	8.08	8.02	0.025	0.027

corresponding to parameters t in Eq. (2) are described by the Slater-Koster rules [14].

***sp-d* Exchange interaction**

When a semiconductor contains localized magnetic ions such as Mn^{2+}, their magnetic moments will interact with carriers and alter an energy level near the band edge. The exchange interaction H_{ex} can be expressed as the Heisenberg Hamiltonian [15]:

$$H_{ex} = -\sum_{\vec{R}_i} J(\vec{r}-\vec{R}_i)\,\hat{\sigma}\cdot\hat{S}_i \qquad (3)$$

where $\hat{S}_i$ and $\hat{\sigma}$ are spin operators of $Mn^{2+}$and carriers, respectively. Here, J is the exchange coupling constant between carrier and magnetic ions; $\vec{r}$ and $\vec{R}_i$ are coordinates of the band electron and Mn^{2+}, respectively. The summation is taken over the number of magnetic ions.

Using the mean field approximation, H_{ex} can be simplified and much easier to implement with the tight-binding calculation. This approach has been successfully used by many researchers [8], [9], [10]. In this approximation, the spin operator of a magnetic ion $\hat{S}_i$ is replaced by $\langle\hat{S}\rangle$, which is the thermal average spin of all Mn ions. For a paramagnetic system, if the Mn ions are magnetized by an applied magnetic field in the *z*-direction, $\langle\hat{S}\rangle$ will have only the z-component $\langle S_z\rangle$, which is the mean spin value per Mn ion. It can be experimentally described by the Brillouin function B_s [16], as shown in Eq. (4).

$$\langle S_z\rangle = S_0 B_s\left(\frac{g\mu_B SB}{k_B(T-T_0)}\right) \qquad (4)$$

where g = 2 is the g-factor of magnetic ions; and S =5/2 is the Mn spin value. As usual, μ_B, k_B, B and T are Bohr magneton, Boltzmann constant, applied magnetic field strength and temperature, respectively. The parameters S_0 and T_0 are effective spin saturation value and temperature correction. These parameters depend on the Mn mole fraction *x*, number of

magnetic ion per cation. Consequently, the exchange Hamiltonian takes a form of Eq. (5), and it can be directly added to the original Hamiltonian H_{TB}

$$H_{ex} = -N_0 x \sigma_z \langle S_z \rangle J \quad (5)$$

We note here that N_0 is the total number of cations per unit volume, and the exchange integrals for the s-like and p-like spatial coordinates are expressed by $\alpha = \langle s|J|s\rangle$ and $\beta = \langle p_x|J|p_x\rangle = \langle p_y|J|p_y\rangle = \langle p_z|J|p_z\rangle$, respectively. These model parameters can be extracted by matching computational and experimental results.

The exchange integral parameters for Mn-doped II-VI DMS are referenced from Ref. [16], where we have chosen $N_0\alpha = 0.26$ eV and $N_0\beta = -1.31$ eV. In low doping concentration, the effective spin saturation value S_0 is $5/2$, following the experimental value [17].

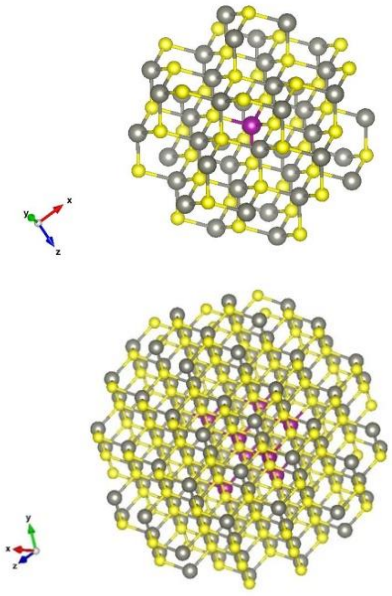

Figure 1. ZnS nanocrystals of different sizes (left: 1.6 nm, right 2.6 nm) with 1% Mn-doped. Mn, Zn and S atoms are displayed in purple, yellow and grey, respectively.

Computation details and procedure

A tight-binding program based on the $sp^3d^5s^*$ orbital bases has been successfully employed in simulations. Full details description of the code can be found in Refs. [18-19]. In this work, we further implement the PRIMME model (see Refs.[20-21] to diagonalize the empirical tight-binding matrix. Since the single-particle spectra are numerically obtained, the electronic structures are analyzed and compared. Next, the eigvenvalues and eigenfunctions computed from the tight-binding model are processed by Matlab code to compute important physical quantities such as DOS.

Results and discussion

In this section, we present and discuss our results on the electronic structure of properties of Mn-doped ZnS. To that end, we benchmark our results with other methods in case of undoped ZnS and Mn-doped ZnS. With Mn-doped ZnS, we include the *sp-d* exchange interaction, and the results on the DOS are reported and discussed in Section 4.2.

Mn-doped and undoped ZnS Benchmarked Results with other Methods

ZnS nanocrystals are constructed to be a spherical shape with the zinc blende structure. The substitution of Mn atoms occurs at the central site, as shown in figure 1, corresponding to an observation from experiment [13]. Our simulation results of band gaps agree well with those from Ref. [22], in which their results are also consistent with experiment; see figure 2 (left). This indicates that our simulation program is reliable. For 1% Mn-doped ZnS, figure 2 (right) shows that the band gaps from tight-binding model are in the same trend with the experimental results [6]. With the increasing size, the reduction of the band gaps is realized due to the quantum confinement effect.

In addition, we investigate the impact of the Mn concentrations on the band gaps. As evident in figure 3, the band gaps decrease with the increasing Mn doping concentrations (%). This trend is consistent with the experimental results [7], though our results yield a relatively small change of the band gaps. We remark here that the possible causes of the minor change and discrepancy between the tight-binding and experimental results are being investigated, and we believe that atomic relaxation could be one of such causes. In experiment, the atomic positions, hence lattice constant, in the nanocrystal are determined naturally. In the present work, a structural relaxation is numerically ignored, and the nanocrystals are always assumed to maintain the same lattice constant even after doping.

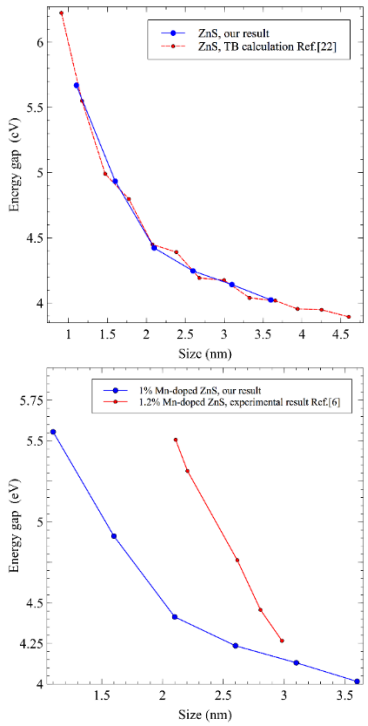

Figure 2. Comparison of energy gap of ZnS (without doping) with other simulation results (left); and of 1% Mn-doped ZnS with experimental results from Ref. [6] (right).

Mn-doped ZnS including exchange interaction

The *sp-d* exchange interaction is taken into account when the system contains magnetization, as the magnetization directly determines the mean spin value $\langle S_z \rangle$, which is our input, by Brillouin function in Eq. (4),

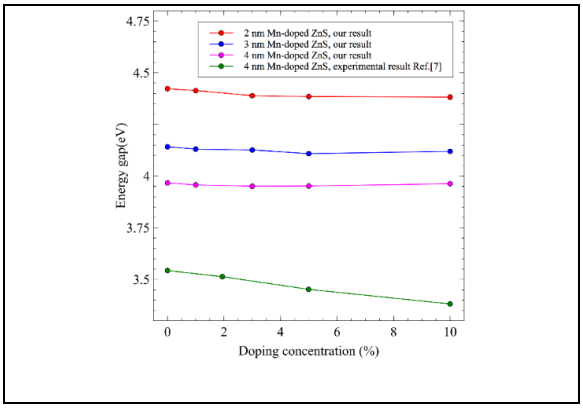

Figure 3. Effect of doping concentration on energy gaps in the comparison with experiment results from Ref. [7].

In this work, we limit our study on the maximum magnetization, which is $\langle S_z \rangle = S_0$. The effect of the *sp-d* exchange interaction will be further analyzed by DOS, shown in figure 4. When we ignore the *sp-d* exchange interaction, the DOS of spin up and spin down are symmetric in every size, as shown by the dashed lines. When we consider the *sp-d* exchange interaction between localized magnetic ions and carriers, the DOS is no longer symmetric (solid lines) as can be clearly seen in figure 4 (top left). With the increasing diameter of ZnS nanocrystals, the DOS becomes more symmetric, meaning that the magnetic property is gradually reduced. Therefore, the magnetic behavior is manipulated by nanocrystal sizes.

Conclusion

We have performed empirical tight-binding calculation to investigate the electronic structure and density of states of Mn-doped ZnS nanocrystals. Our simulations are benchmarked consistently with other simulation and experimental results. The computations underlying the electronic structures mainly depend on the diameters and Mn atoms. With the increasing size of the ZnS nanocrystals, the reduction of the band gap energy is exhibited because of the quantum confinement effect. As can be seen, the band gaps decrease with the increasing Mn doping concentration. In the presence of the *sp-d* exchange interaction between localized magnetic ions and carriers, the DOS is no longer symmetric. With the increasing diameters of ZnS nanocrystals, the magnetic property is gradually reduced. Therefore, the electronic and magnetic properties are significantly controlled by the size of the nanocrystals and Mn concentrations.

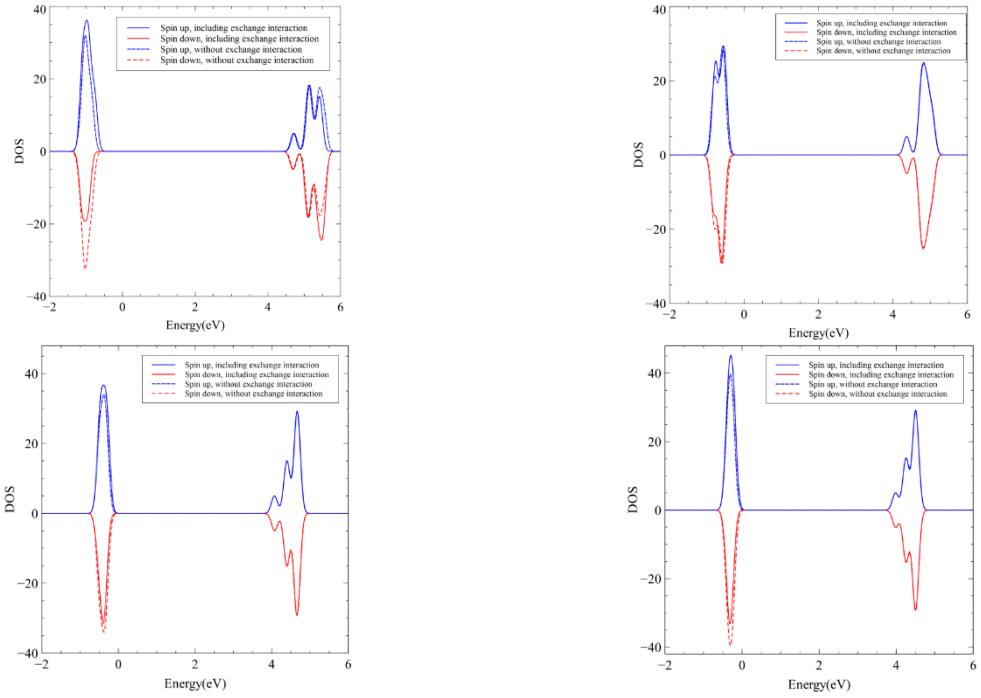

Figure 4. Density of states (DOS) of 1% Mn-doped ZnS comparing with undoped ZnS with different sizes are shown. The nanocrystal diameters are 1.1 nm (top left), 1.6 nm (top right), 2.1 nm (bottom left) and 2.6 nm (bottom right). DOS are calculated from 20 lowest energy electron and holes states broadened by Gaussian function with σ = 0.08 eV.

Acknowledgments

R. Hunkao would like to thank the Development and Promotion of Science and Technology Talents (DPST) project for a scholarship to study at Faculty of Science, Mahidol University. W. Sukkabot acknowledges financial support from the Thailand Research Fund Grants (TRG58880072).

References

[1] Wu, P. et al., 2010. "Conjugation of Glucose Oxidase onto Mn-Doped Zns Quantum Dots for Phosphorescent Sensing of Glucose in Biological Fluids". **Analytical Chemistry.** 82: 1427-1433.

[2] Adegoke, O.; Park, E. Y., 2016. "Size-Confined Fixed-Composition and Composition-Dependent Engineered Band Gap Alloying Induces Different Internal Structures in (L)-Cysteine-Capped Alloyed Quaternary Cdzntes Quantum Dots". **Scientific Reports.** 6: 27288.

[3] Saïdi, I. et al., 2016. "Optical Properties of Type-Ii Alinas/Algaas Quantum Dots by Photoluminescence Studies". **Journal of Applied Physics.** 120: 035701.

[4] Bailey, R. E.; Nie, S., 2003. "Alloyed Semiconductor Quantum Dots: Tuning the Optical Properties without Changing the Particle Size". **Journal of the American Chemical Society.** 125: 7100-7106.

[5] Zhang, J. Z. et al., 2014. "Rational Codoping as a Strategy to Improve Optical Properties of Doped Semiconductor Quantum Dots". **The journal of physical chemistry letters.** 5: 3694-3700.

[6] Chandrakar, R. K. et al., 2015. "Synthesis, Characterization and Photoluminescence Studies of Mn Doped Zns Nanoparticles". **Superlattices and Microstructures.** 86: 256-269.

[7] Mote, V. et al., 2013. "Structural, Morphological and Optical Properties of Mn Doped Zns Nanocrystals". **Cerâmica.** 59: 614-619.

[8] Guo, Y. et al., 2012. "A Tunable Spin Filter in Periodic Diluted Magnetic Semiconductor/Semiconductor Superlattices". **Applied Physics Letters.** 101: 012410.

[9] Olbrich, P. et al., 2012. "Spin-Polarized Electric Currents in Diluted Magnetic Semiconductor Heterostructures Induced by Terahertz and Microwave Radiation". **Physical Review B.** 86: 085310.

[10] Yang, W. et al., 2006. "Spin-Polarized Transport in a Lateral Two-Dimensional Diluted Magnetic Semiconductor Electron Gas". **Applied Physics Letters.** 88: 082107.

[11] Papaconstantopoulos, D.; Mehl, M., 2003. "The Slater–Koster Tight-Binding Method: A Computationally Efficient and Accurate Approach". **Journal of Physics: Condensed Matter.** 15: R413.

[12] Gürel, H. H. et al., 2008. "Tight Binding Modeling of Cdse/Zns and Cdzns/Cds Ii–Vi Heterostructures for Solar Cells: Role of D-Orbitals". **Thin Solid Films.** 516: 7098-7104.

[13] Albe, V. et al., 1998. "Electronic Structure of Mn-Doped Zns Nanocrystals". **Physical Review B.** 57: 8778.

[14] Slater, J. C.; Koster, G. F., 1954. "Simplified Lcao Method for the Periodic Potential Problem". **Physical Review.** 94: 1498.

[15] Furdyna, J. K., 1988. "Diluted Magnetic Semiconductors". **Journal of Applied Physics.** 64: R29-R64.

[16] Gaj, J. A.; Kossut, J. 2011. **Introduction to the Physics of Diluted Magnetic Semiconductors.** Springer Science & Business Media, Vol. 144.

[17] Fatah, J. et al., 1994. "Numerical Simulation of Antiferromagnetic Spin-Pairing Effects in Diluted Magnetic Semiconductors and Enhanced Paramagnetism at Interfaces". **Physical Review B.** 49: 10341.

[18] Sukkabot, W., 2014. "Tight-Binding Theory of the Excitonic States in Colloidal Insb Nanostructures". **Materials Science in Semiconductor Processing.** 27: 51-55.

[19] Sukkabot, W., 2015. "Role of Structural and Compositional Details in Atomistic Tight-Binding Calculations for Inn Nanocrystals". **Materials Science in Semiconductor Processing.** 38: 142-148.

[20] Stathopoulos, A.; McCombs, J. R., 2010. "Primme: Preconditioned Iterative Multimethod Eigensolver&Mdash;Methods and Software Description". **ACM Trans. Math. Softw.** 37: 1-30.

[21] Wu, L. et al., 2016. "Primme_Svds: A High-Performance Preconditioned Svd Solver for Accurate Large-Scale Computations". **arXiv preprint arXiv:1607.01404.**

[22] Lippens, P.; Lannoo, M., 1989. "Calculation of the Band Gap for Small Cds and Zns Crystallites". **Physical Review B.** 39: 10935.